J. Synchrotron Rad. (1997). **4**, 155–162

Compression Behaviour of Elastically Anisotropic Polycrystals Using Energy-Dispersive X-ray Diffraction

J. W. Otto,[a] J. K. Vassiliou[b] and G. Frommeyer[a]

[a]Max-Planck-Institut für Eisenforschung, Max-Planck-Strasse 1, 40237 Düsseldorf, Germany, and [b]Department of Physics, Villanova University, Villanova, PA 19085, USA. E-mail: jenso.pzb@metronet.de

(Received 22 November 1996; accepted 21 March 1997)

The compression behaviour of a foil of Cu_3Au in a pressure medium of NaCl has been studied by energy-dispersive X-ray diffraction in a diamond-anvil cell. Evidence from stress analysis and peak broadening of the foil (the most extreme example of a non-ideal powder) throws light on the compression of powders under non-hydrostatic conditions. A complete pressure cycle, including re-pressurization after pressure release, shows that significant plastic deformation takes place which results in large deviations from a (hydrostatic) equation of state. The origin of the deformations is traced to shear stresses transmitted to the sample through the pressure medium.

Keywords: high pressure; Cu_3Au; equation of state; plastic deformation; polycrystals.

1. Introduction

One of the fundamental problems in high-pressure research is how to ensure the hydrostatic environment necessary for the study of physical parameters. Pressure devices such as the diamond-anvil cell do not generate an isotropic macroscopic stress field and pressure-transmitting media may transmit significant shear stresses due to either an increase in viscosity (shear strength) or solidification under pressure. Elastically anisotropic polycrystalline samples set up localized (micro)stresses even in a hydrostatic environment due to grain boundaries between crystals with randomly oriented hard and soft directions. Among the evidence for non-hydrostatic conditions documented with X-ray scattering are deviations in the compression data V/V_0 *versus* pressure from equations of state which are based, at the low pressures considered here, on the theory of finite strain for elastic bodies (Birch, 1938). A discontinuity in the compression curve of MgO embedded in NaCl was identified by Sato, Yagi, Ida & Akimoto (1975) as the yield point of MgO. The yield point marks the transition from elastic to plastic behaviour and is observed as a deviation from a linear relation between stress and strain. No evidence was presented by the above authors for plastic deformation which should occur when stresses exceed the flow stress above the yield point. A saturation in strains and uniaxial stresses calculated from lattice spacings (Singh & Kennedy, 1976; Kinsland & Bassett, 1977) and Gaussian peak widths (Singh, Vijayan, Xia, Vohra & Ruoff, 1992; Vassiliou, Otto & Porter, 1994; Weidner, Wang, Meng & Vaughan, 1994*a*) was identified as the yield point of the sample. The reversibility with pressure of the strains was not investigated in previous X-ray studies and hence both the origin and the location of the yield point remain ambiguous. We have initiated a systematic study of the effect of different pressure devices (MAX80, diamond-anvil cell), pressure-transmitting media (NaCl, paraffin oil and 4:1 methanol–ethanol) and sample strength on the compression behaviour of polycrystals. This work, which presents an analysis of compression data for a foil of Cu_3Au embedded in NaCl in a diamond-anvil cell, is presented as a first step in filling this gap.

2. Methodology

2.1. *Choice of sample and pressure device*

The requirements on the sample are sensitivity to (shear) stresses and small crystallite size (of the order of 1 μm) for powder averaging in energy-dispersive diffraction with a diamond-anvil cell. The sensitivity to shear stresses (and hence ductility) is governed by the availability of five independent sets of slip planes (von Mises criterion). In the cubic $L1_2$ structure, these are the {111} planes, with slip on {001} also being possible (Yamaguchi & Umakoshi, 1990). We chose to investigate disordered Cu_3Au because (i) it remains ductile even at liquid-nitrogen temperatures and hence no brittle-to-ductile transition was expected under pressure, (ii) it has strong X-ray reflections, and (iii) it is possible to produce a microcrystalline foil by splat-quenching. A foil is expected to be particularly sensitive to stresses because grain boundaries can act as local sources of stress (due to pile-up of dislocations). It is the 'worst possible case' of the compression of non-ideal powder.

A diamond-anvil cell was chosen here as a pressure-generating device since it produces a uniaxial stress field (the stress along the compression axis, σ_3, being greater than the radial stress, σ_1) which should lead to shear stresses on the sample if (when) the pressure-transmitting medium becomes non-hydrostatic. A Holzapfel-type cell (Syassen &

Holzapfel, 1975) was used with a maximum opening angle of $2\theta = 11.4°$. The diffraction angle was $\theta = 5.39°$ in this study.

NaCl was used as a pressure-transmitting medium. Evidence from line broadening of fluorescence spectra from ruby embedded in NaCl suggests that NaCl transmits significant shear stresses at low pressures (around 5 GPa; Piermarini, Block & Barnett, 1973). NaCl also serves as a pressure calibrant in addition to ruby. Pressures were calculated from the volume data of NaCl using the equation-of-state parameters $B_0 = 24.008$ GPa and $B_0' = 4.74$ obtained from a fit to the data of Decker (1971), and from the line shift of the ruby fluorescence (Mao, Bell, Shaner & Steinberg, 1978).

The samples were prepared as follows. NaCl was ground and then dried and annealed at 383 K. Samples were placed inside the 150 μm hole in a 70–80 μm-thick spring steel gasket. Two flakes of Cu_3Au were carefully removed from the 20–50 μm-thick foil and sandwiched between two layers of NaCl. A single grain of ruby of size 5–10 μm was embedded in the NaCl in the (horizontal) centre of the gasket hole. Care was taken to ensure that (i) the flakes were of much smaller diameter than the gasket hole so that no contact occurred with the gasket during the experiment; (ii) the flakes were lying flat in the cell to avoid bridging between the diamonds; (iii) no contact occurred between ruby and either foil or diamonds. During the course of the experiment, diffraction peaks from NaCl were always observed demonstrating that the foil made no contact with the diamonds. This is confirmed by the observation of colour defects on both sides of the foil caused by the X-ray beam passing through NaCl. The gasket hole collapsed to a diameter of 80 μm by 2.9 GPa and expanded to its original diameter of 150 μm by 11.1 GPa starting at around 5.8 GPa.

It is important to realize that, with the set-up employed, the pressure determined from ruby and from NaCl under hydrostatic conditions is the confining pressure on the sample. This may be different from the pressure the sample itself experiences (see below). The pressure determined from ruby is labelled as confining pressure on all graphs.

2.2. *Calculating stresses from observed strains*

Using anisotropic elasticity theory, Singh & Kennedy (1974) have shown that the total strain, ε, in a diffraction experiment depends on the direction in the lattice in which it is being measured:

$$\begin{aligned}\varepsilon^{\text{total}}(hkl) &= \varepsilon^p + \varepsilon^t(hkl) \\ &= [d(hkl) - d_0(hkl)]/d_0(hkl), \end{aligned} \quad (1)$$

where p denotes the component due to hydrostatic pressure, t the component due to uniaxial stress, and $d(hkl)$ is the measured lattice spacing. For a sample in an opposed-anvil device with the incident beam along the compression axis, Singh (1993) has shown that the measured strain is related to the uniaxial stress, $t = \sigma_3 - \sigma_1$, and the elastic anisotropy factor $S = S_{11} - S_{12} - 0.5S_{44}$, as

$$\begin{aligned}\varepsilon^{\text{total}}(hkl) &= \sigma_p/3K + (1-\alpha)\varepsilon_d^V + \alpha\varepsilon_d^R \\ &= \sigma_p/3K - (1-\alpha)(t/3)(1 - 3\sin^2\theta)/2\mu_V \\ &\quad - \alpha(t/3)(1 - 3\sin^2\theta)(S_{11} - S_{12} - 3S\Gamma), \end{aligned} \quad (2)$$

where V denotes the Voigt state (strain continuity), R the Reuss state (stress continuity), α the fraction of the Reuss state actually present in the sample, K the bulk modulus, μ the shear modulus, and the geometrical factor $\Gamma = (h^2k^2 + k^2l^2 + h^2l^2)/(h^2 + k^2 + l^2)^2$. For a constant angle θ, as is used in energy-dispersive diffraction, the stress can be calculated from the slope of the measured strains *versus* Γ if the elastic constants and the factor α are known as a function of pressure. For isotropic solids the anisotropy factor $S = 0$ or

$$2(S_{11} - S_{12})/S_{44} = 1$$

and $\mu_V = \mu$. Therefore,

$$\varepsilon_d^R = \varepsilon_d^V.$$

Using the relation

$$\varepsilon^p = \sigma^p/3K = P^R/3K,$$

valid for cubic solids, where P^R denotes the hydrostatic pressure, and identifying

$$P^M = 3\varepsilon^{\text{total}}(hkl)K,$$

where P^M is the measured pressure, we can calculate, for isotropic solids, the real pressure from the measured pressure as

$$P^R = P^M - (\sigma_3 - \sigma_1)(K/2\mu)(1 - 3\sin^2\theta), \quad (3)$$

where μ is the shear modulus $1/[2(S11 - S12)]$. For anisotropic solids the second term in the above equation needs to be multiplied by the factor

$$(1-\alpha)\mu/\mu_V + \alpha 2\mu(S_{11} - S_{12} - 3S\Gamma).$$

For the {100} family of lattice planes, $\Gamma = 0$ and this factor simplifies to

$$(1-\alpha)\mu/\mu_V + \alpha.$$

In the calculations presented below, the elastic constants for NaCl were calculated from the values and their pressure derivatives determined up to 0.8 GPa by Spetzler, Sammis & O'Connel (1972). The elastic constants of disordered Cu_3Au were determined at 1 atm by Siegel (1940). For the pressure derivatives the values of Cu and Au weighted by the appropriate stoichiometric ratio were used since the elastic constants calculated in this way at 1 atm do not differ much from those determined directly on Cu_3Au.

2.3. *Experimental set-up*

For the powder-diffraction method, energy-dispersive diffraction at a synchrotron source was chosen. In the energy-dispersive method the diffraction angle θ is kept

constant (reciprocal lattice vectors being selected by the different wavelengths in the white beam). A high brilliance of the primary beam was necessary for the small samples; this was especially important in the present case since the deformation of the sample caused strong peak broadening and increased diffuse scattering, leading to very long counting times. A low-divergence source was required in order to have both the resolution and the peak profile to be determined only by the detector electronics. The experiments were carried out at beamline F3 at Hamburger Synchrotron Strahlungslabor at Deutsches Elektronen Synchrotron with the set-up described by Otto (1997*a*). Using a small primary beam (40 × 40 μm) and tight collimation of the diffracted beam in both the horizontal and vertical directions, the resolution function can be parametrized in the following way in the angular range used here:

$$\Delta E/E = [(0.154)^2/E^2 + (5.546 \times 0.10 \times \varepsilon)/E]^{1/2},$$

where the Fano factor $F = 0.10$ and the resolution of the amplifier is $\Delta E_{amp} = 0.154$ keV (Otto, 1997*b*). Keeping the deadtime of the detector below 5%, the peak shape for the NBS640B silicon standard was determined to be better than 95% Gaussian (Otto, 1997*b*). The peak profile of polycrystals under pressure has not been investigated before.

3. Results

3.1. *Stress and strain from lattice spacings*

Uniaxial stresses should lead to deviations in $(V/V_0)(hkl)$ calculated from the individual lattice spacings [see equation (2)]. This is illustrated in Fig. 1 for the Cu_3Au foil with increasing confining pressure to 6 GPa. $(V/V_0)(hkl)$ calculated from the five different lattice planes observed (Table 1) is seen to diverge strongly immediately on compression. However, the compression behaviour for all lattice planes follows the same trend. High initial compressibility to 1 GPa is followed by hardening to 2 GPa. $(V/V_0)(hkl)$ remains constant for confining pressures between 2 and 4 GPa and decreases above 4 GPa at a rate of the same order of magnitude as the initial one. The values of $(V/V_0)(hkl)$ at any pressure calculated from the (111), (220) and (222) reflections are quite similar and show the highest compressibility, while those from (200) show the lowest compressibility, with the values for (311) lying in between or close to (200). This behaviour is expected from the anisotropy parameter S for the lattice planes under elastic compression, as pointed out by Meng, Weidner & Fei (1993) [see also equation (2)]. In order to represent the compression behaviour more clearly for the complete experiment and to facilitate comparison with experiments using different pressure media, the volume average $(\bar{V}/\bar{V}_0)$ is plotted for increasing pressure (open circles), pressure release (solid circles) and second pressurization (solid squares) in Fig. 2. The significant strains seen in Fig. 1 are represented here as error bars calculated for $(V/V_0)(200) - (\bar{V}/\bar{V}_0)$ and $(\bar{V}/\bar{V}_0) - (\bar{V}/\bar{V}_0)(111 + 220 + 222)$. The compression curve for the scaled average volume follows the trend of that calculated from the individual lattice planes. The release curve down to 2 GPa lies on or close to the curve for pressure increasing above 4 GPa. At pressures below 2 GPa the hysteresis loop seems to close. Hence, there is a pressure region on both pressure increase and pressure release over which the volume does not change (this is not clearly seen on pressure release because of the experimental difficulty of controlling and measuring the pressure at such low loads). On increasing pressure for the second time on the same

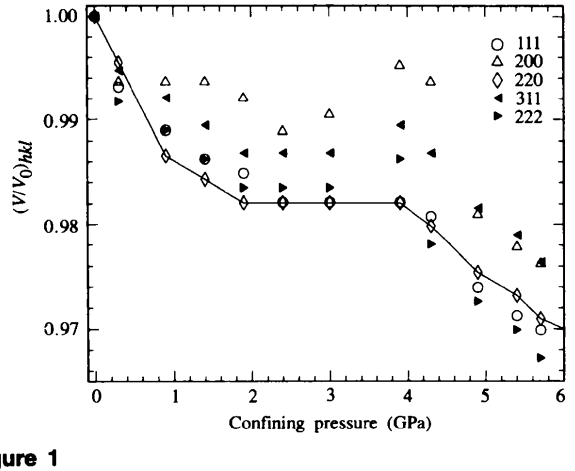

Figure 1
Plot of $V/V_0(hkl)$ *versus* pressure for the five different lattice planes of Cu_3Au observed in this experiment. The solid line connects V/V_0 calculated from the (220) plane to illustrate the general trend also followed by V/V_0 calculated from the other lattice planes. The (200) plane is the one most sensitive to shear stresses.

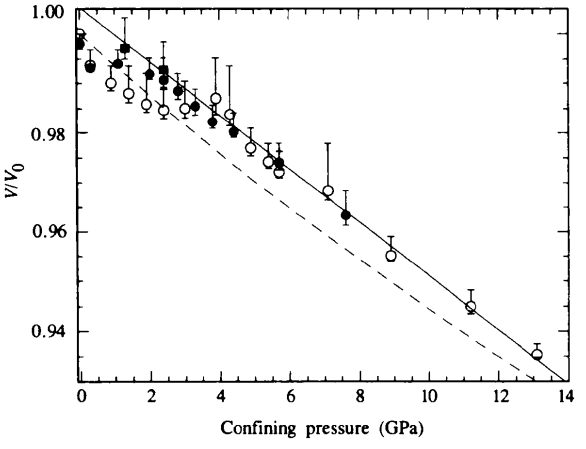

Figure 2
The average volume $(\bar{V}/\bar{V}_0)$ calculated from the five observed lattice planes of Cu_3Au *versus* pressure. Open symbols are for increasing confining pressure, solid circles for pressure release and solid squares for second pressurization. The error bars represent $(\bar{V}/\bar{V}_0)(200) - (\bar{V}/\bar{V}_0)$ and $(\bar{V}/\bar{V}_0) - (\bar{V}/\bar{V}_0)(111 + 220 + 222)$. The solid line is a fit to the increasing pressure values above 4 GPa. Note that the release curve follows this trend down to about 2 GPa, where the volume hysteresis loop begins to close. The dashed curved is the first-order Birch–Murnaghan equation of state calculated from the elastic constants determined by Siegel (1940).

sample the compression curve follows the previous release curve and not the initial compression curve.

For discussing the stresses calculated from the observed strains using equation (2), we assume the Reuss condition of stress continuity [the value of α cannot be determined with the scattering geometry used; see Funamori, Yagi & Uchida (1994)]. The uniaxial stress (negative in compression) in Cu_3Au increases immediately on compression (Fig. 3*a*), seems to pass through a maximum of 1 GPa near 4 GPa and to decrease above this pressure. It is not clear whether there is an actual decrease or whether the values saturate above 4 GPa. On pressure release (Fig. 3*b*) the stresses do not relax completely: the residual compressive stress is 0.3 GPa. On second pressurization the stresses at 1.3 and 2.5 Pa lie close to the maximum value of the first pressure cycle (Fig. 3*b*). The stress curve for NaCl shows a saturation in the range 3–4 GPa (Fig. 4*a*). As expected, the maximum stress is much lower than for Cu_3Au (~0.4 GPa compared with 1 GPa). The stresses in NaCl relax completely with a slight hysteresis between 4 and 1 GPa (Fig. 4*b*). The pressures calculated from the lattice parameters of NaCl (without correction for the uniaxial stresses) and from the ruby fluorescence agree very well (Fig. 5), as expected from the rather small stresses calculated for NaCl. There appears to be a weak trend in the compression curve for NaCl similar to that seen in Cu_3Au. Higher resolution of both the X-ray method and the spectrometer for recording the ruby fluorescence would be required to reach a definite conclusion on this point.

3.2. *Peak profiles*

In the analysis of the diffraction spectra it was noted that the r values of Gaussian fits to the Bragg reflections of Cu_3Au deteriorated with increasing pressure. The poor Gauss fit and the very much improved Voigt fit to the triplet of Cu_3Au (111), NaCl (220) and Cu_3Au (200) after the first

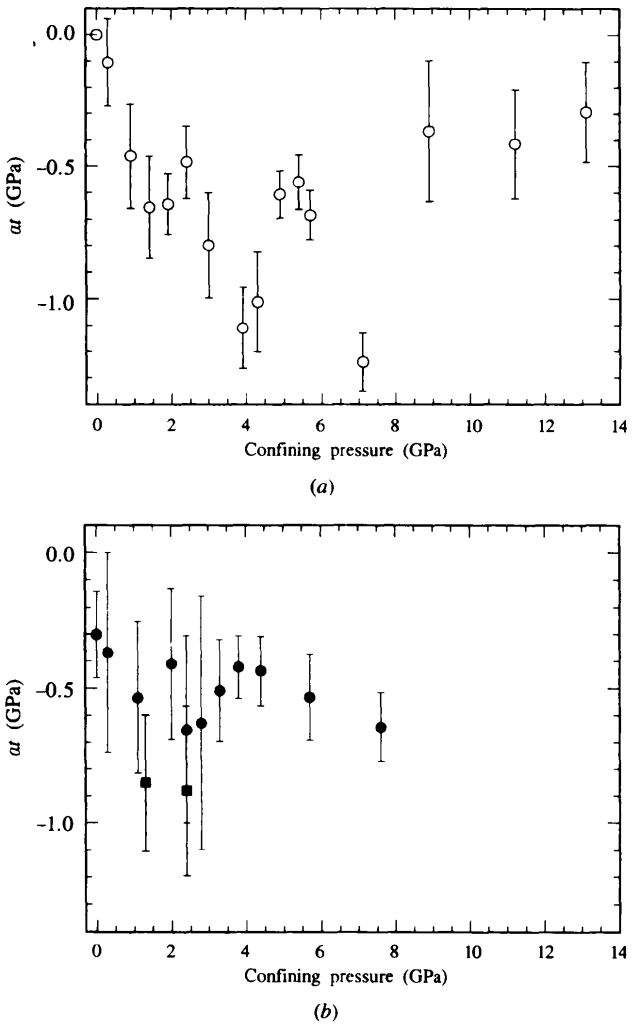

Figure 3
The product αt [fraction of Reuss state in the sample times the stress calculated according to equation (2)] for Cu_3Au with increasing confining pressure (*a*) and pressure release (solid circles) and second pressurization (solid squares) (*b*). Note the residual stress of 0.3 GPa. The error bars are from the fit to $d\varepsilon/d\Gamma$ [equation (2)].

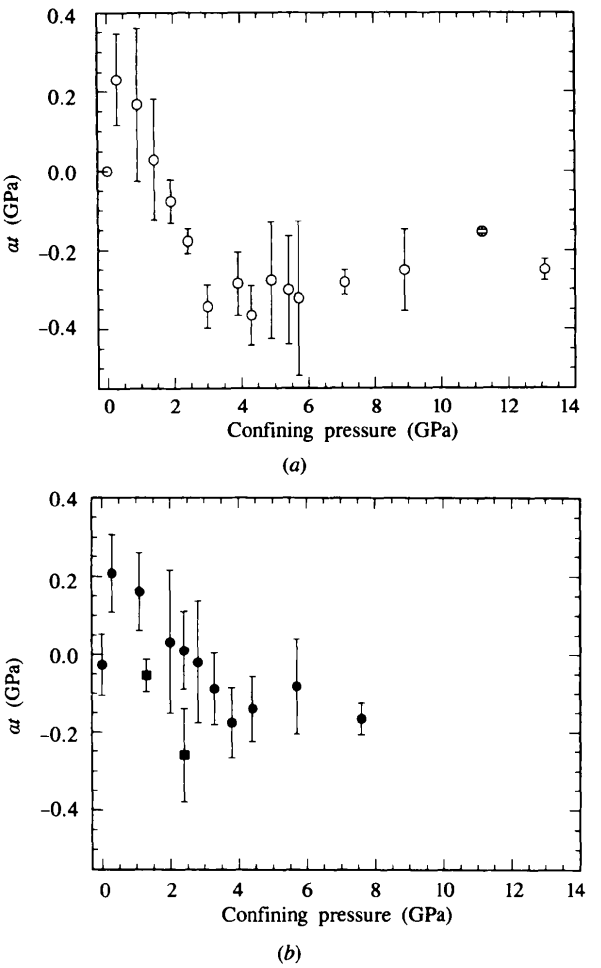

Figure 4
(*a*), (*b*) Same as Fig. 3 for NaCl. Note the closed hysteresis loop (complete stress relaxation) which is in the sense opposite to the one expected. We do not have an explanation for the positive values of the stress seen at the lowest pressures during the first pressure cycle. The parameter S does not change sign to at least 0.8 GPa (Spetzler, Sammis & O'Connel, 1972)

Table 1
Lattice parameter, V/V_0 and d spacings as a function of pressure determined from NaCl and ruby.

Pressure (GPa) (NaCl)	Pressure (GPa) (ruby)	Lattice parameter (Å)	V/V_0	d spacings (Å) 111	200	220	311	222
0.0001	0.0001	3.759	1.000	2.170	1.878	1.330	1.133	1.086
0.3	0.3	3.751	0.994	2.165	1.874	1.328	1.131	1.083
1.0	0.9	3.747	0.990	2.162	1.874	1.324	1.130	1.082
1.5	1.4	3.744	0.988	2.160	1.874	1.323	1.129	1.081
1.9	1.9	3.743	0.987	2.159	1.873	1.322	1.128	1.080
2.4	2.4	3.739	0.984	2.157	1.871	1.322	1.128	1.080
2.9	3.0	3.741	0.986	2.157	1.872	1.322	1.128	1.080
3.4	3.9	3.743	0.987	2.157	1.875	1.322	1.129	1.081
4.0	4.3	3.740	0.985	2.156	1.874	1.321	1.128	1.078
4.9	4.9	3.729	0.976	2.151	1.866	1.319	1.126	1.076
5.3	5.4	3.726	0.974	2.149	1.864	1.318	1.125	1.075
5.8	5.7	3.724	0.972	2.148	1.863	1.317	1.124	1.074
6.8	7.1	3.717	0.967	2.144	1.864	1.315	1.122	1.072
9.1	8.9	3.702	0.955	2.136	1.852	1.309	1.117	1.068
11.1	11.2	3.689	0.945	2.128	1.845	1.304	1.114	1.064
13.2	13.1	3.677	0.936	2.122	1.838	1.300	1.110	1.060
7.5	7.6	3.712	0.963	2.141	1.858	1.312	1.120	1.072
5.3	5.7	3.726	0.974	2.150	1.864	1.317	1.124	1.076
4.2	4.4	3.734	0.980	2.155	1.868	1.320	1.126	1.078
3.8	3.8	3.736	0.982	2.156	1.869	1.321	1.127	1.079
3.4	3.3	3.740	0.985	2.158	1.871	1.322	1.129	1.080
2.9	2.8	3.745	0.989	2.161	1.873	1.323	1.131	1.080
2.4	2.4	3.748	0.991	2.163	1.875	1.324	1.130	1.082
1.9	2.0	3.749	0.992	2.164	1.875	1.325	1.130	1.083
1.3	1.1	3.752	0.994	2.167	1.876	1.326	1.131	1.083
0.7	0.3	3.750	0.993	2.166	1.876	1.327	1.129	1.083
0.0001	0.0	3.756	0.998	2.168	1.878	1.328	1.133	1.085
1.3	1.3	3.755	0.997	2.166	1.880	1.327	1.133	1.084
2.5	2.4	3.750	0.993	2.163	1.877	1.325	1.132	1.082

pressure cycle is illustrated in Fig. 6 [Voigt fit (top), residuals for Voigt fit (middle) and for Gauss fit (bottom)]. Note that the Voigt fit for NaCl (220) is no improvement over the Gauss fit. For the Cu_3Au diffraction peaks the Gauss curve fails to fit the tails and the peak centre, resulting in a significant underestimation of integrated intensity. Voigt fits were employed for both Cu_3Au and NaCl in all spectra. The high background due to diffuse scattering, the peak broadening (see below) and peak overlap especially between NaCl (220) and Cu_3Au (200) under pressure resulted in strong scatter in the Lorentzian and Gaussian fractions and half-widths calculated from the Voigt fit parameters. Hence, no detailed analysis of the pressure dependence of these parameters was possible. [In the experiments with liquid transmission media, backgrounds were much lower, and such analysis will be presented elsewhere (Otto, Vassiliou & Frommeyer, 1997*a*).] However, peak locations and FWHM could be determined reliably and in general did not differ beyond experimental error from the values obtained with Gauss fits.

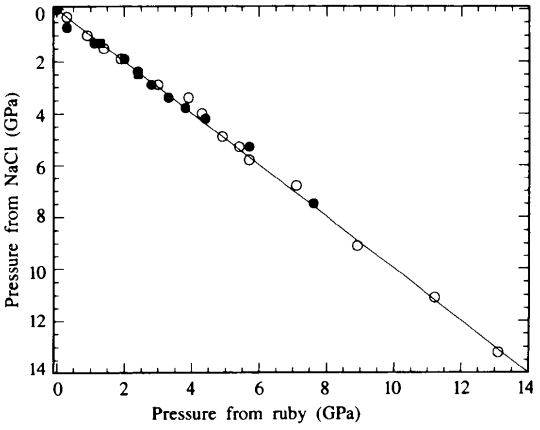

Figure 5
Pressure calculated from the observed lattice spacings of NaCl *versus* confining pressure determined from the fluorescence of ruby embedded in NaCl. Note the excellent overall agreement.

The FWHM of all Bragg reflections observed showed a strong increase even at the lowest pressures (0.3 and 1 GPa) of the initial pressurization. Further trends with increasing and decreasing pressure differ somewhat depending on the reflection. Three representative examples are shown for Cu_3Au (220) (Fig. 7*a*), NaCl (220) (Fig. 7*b*) and NaCl (222) (Fig. 7*c*). The FWHM of Cu_3Au increases up to 1 GPa, decreases slightly to 4 GPa and then increases rapidly to saturate at about 7 GPa. On pressure release the FWHM does not decrease down to 2 GPa, and remains 30% broader than before the experiment at 1 atm. On second application of pressure the FWHM increases towards the value at which it saturated during the first pressure cycle. Apparently, there is no first plateau (or maximum) at low pressures as seen during the first pressure cycle. For NaCl a closed hysteresis loop of small width in pressure is observed (Figs. 7*b* and 7*c*). While the release trend is similar for the (220)

and (222) reflections, there are some differences on first pressurization. In both (220) and (222) there is a saturation in FWHM at 1 GPa. There is a rapid increase between 2 and 4 GPa for (220), and between 2 and 8 GPa for (222), followed by saturation. As for Cu_3Au (220), there does not seem to be a plateau in FWHM at low pressures on second pressurization.

4. Discussion

The presence of residual stress in Cu_3Au foil (Fig. 3*b*) and the broadened peak profiles after pressure release (Fig. 7*a*) show that plastic deformation has taken place. The curves of volume compression, stress and FWHM *versus* pressure of Cu_3Au thus reflect the behaviour due to both elastic and plastic compression and the task is to identify the pressure range over which plastic deformation takes place.

The onset of plastic deformation, the yield point, is marked by plastic flow and a deviation from a linear relation between stress and strain. In the case of work hardening, the flow stress required to maintain plastic flow increases with increasing strain (up to the rupture strength of the material). Yielding (plastic deformation) and work hardening should cause a deviation in (V/V_0) from the equation of state towards higher values of the scaled volume because of the introduction of, and mutual repulsion between, line defects.

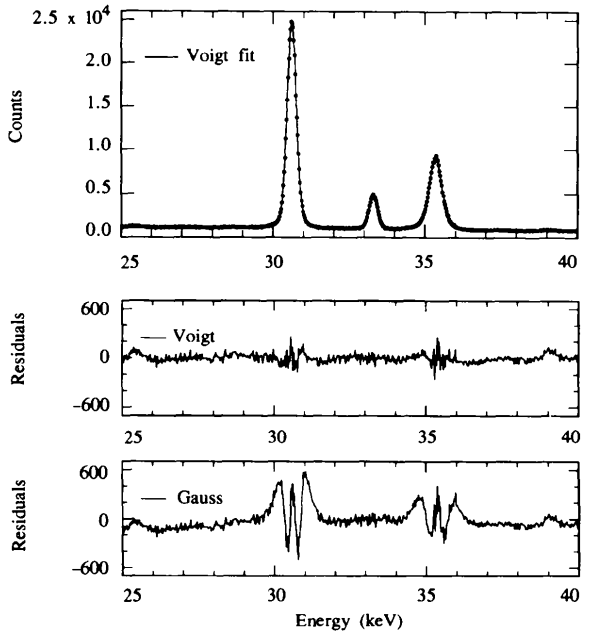

Figure 6
Voigt fit to the diffraction peaks Cu_3Au (111) (left), NaCl (220) and Cu_3Au (200) (right) (top figure), with residuals for the Voigt fit (middle) and a Gauss fit (bottom). Note that the missing intensity in the central and tail sections of the Gauss fit to Cu_3Au indicates a missing Lorentzian component. Hence, the Voigt fit results in a substantially improved r value (r^2 = 0.99976 for the Voigt fit and r^2 = 0.99836 for the Gauss fit). The peak centres from the two fits coincide while there is some difference in the peak widths FWHM (111) = 0.352 (0.362), (200) = 0.486 (0.504), (220) = 0.324 eV (0.323) (the values in parentheses are for the Gauss fits).

In general it can be expected that the initial compression of a polycrystalline material is elastic. The compression curve follows the equation of state when the pressure-transmitting medium is hydrostatic and the polycrystalline aggregate is free from (uniaxial) microstresses. Uniaxial stresses on the sample arise due to increasing shear strength of the pressure-transmitting medium and/or microstresses

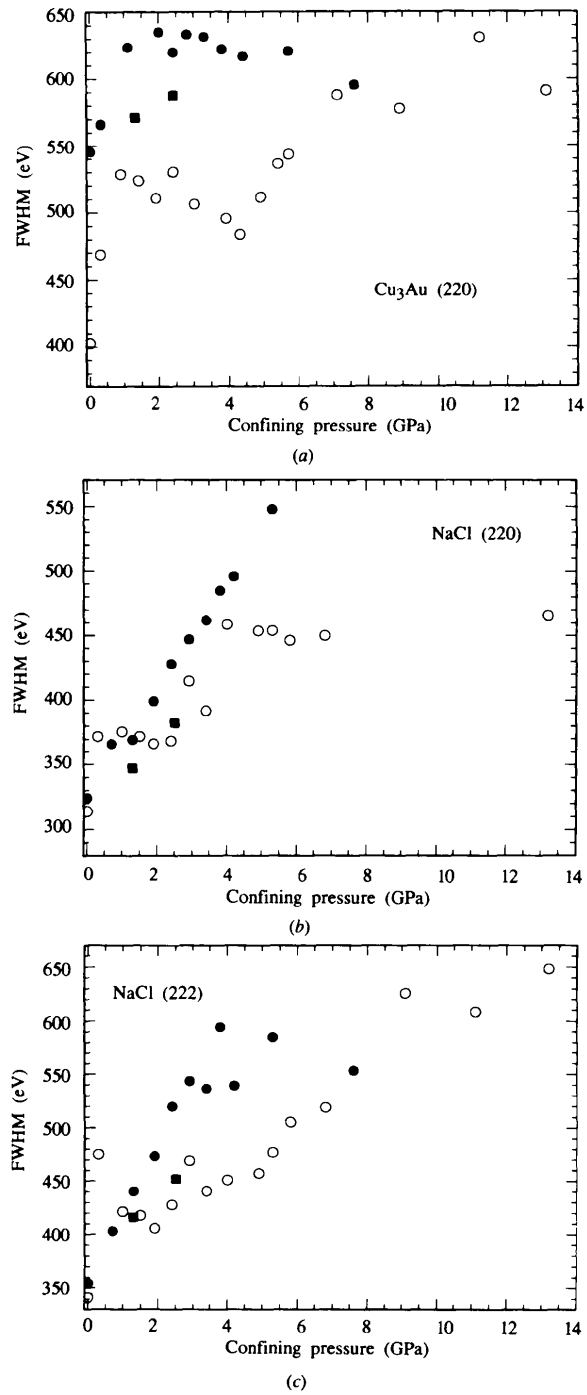

Figure 7
FWHM of Voigt fits to the (220) diffraction peak of Cu_3Au (*a*) and (220) and (222) peaks of NaCl [(*b*) and (*c*), respectively] *versus* confining pressure. Open circles are for increasing pressure, solid circles for pressure release and solid squares for second pressurization.

in the polycrystals. This causes an additional (elastic) compression [equation (3)] resulting in a compressibility higher than would be expected under hydrostatic conditions (stage I). Stage I ends when the external stresses exceed the yield stress of the polycrystalline material. From the saturation of the stresses in the present experiments it can be concluded that the yield points must lie at confining pressures of below 2–4 GPa for Cu_3Au and below 3 GPa for NaCl (Figs. 3*a*, 4*a*). The yield points cannot be detected here because they lie at such low confining pressures that stage I cannot be clearly observed. Note that the shear moduli for NaCl (26 GPa) and Cu_3Au (45 GPa, calculated from the values for Cu and Au weighted by the appropriate stoichiometry) are quite similar, and that the pressure dependence of the shear modulus is higher for NaCl than for Cu_3Au (2.1 *versus* 1.6) (Poirier, 1985). The shear moduli should thus become equal around 1.4 GPa. It is not clear whether the plateau in the FWHM of the NaCl (220) and (222) and Cu_3Au (222) diffraction peaks at around 1 GPa (Figs. 7*a*–7*c*) is related to the yield point. In the initial stages of yielding (work hardening) the foil continues to be compressed elastically (in addition to the plastic deformation taking place). Plastic deformation causes line defects (such as stacking faults) which interact and harden the material (stage II). This region lies between 1 and 2 GPa for Cu_3Au in the present case (Figs. 1 and 2). As the density of defects increases, the (elastic) repulsion between them increases to the extent that no further (elastic) compression can take place: the volume remains constant (at least within the accuracy of the present X-ray method). This stage (stage III) occurs between 2 and 4 GPa (Figs. 1 and 2). Significant deformation takes place [this is clearly seen from the FWHM of the NaCl (220) and (222) but not from the Cu_3Au diffraction peaks (Figs. 7*a*–7*c*)]. When the external pressure overcomes the internal repulsion due to the defects, elastic compression (of a now plastically deformed material) again sets in (stage IV). This causes a discontinuity in the compression curve (Figs. 1 and 2). The FWHM of the diffraction peaks continues to increase above this pressure [Figs. 7*a*–7*c*; the data for NaCl (220) are not reliable above 5 GPa because of overlap with Cu_3Au (200)]. At present it cannot be determined whether the broadening in Cu_3Au is due to increasing strain or decreasing size of coherently diffracting domains or both (the size of the domains decreasing because of the increasing density of dislocations). Saturation in FWHM occurs around 6–8 GPa (Figs. 7*a*–7*c*); there is no anomaly in the compression or stress curves in this range.

On decompression in Cu_3Au the elastic volume strains due to interacting defects stored in the increasing pressure part of the pressure cycle at 1–4 GPa are relaxed in the region 0.5–2 GPa. The plastic strains, however, are not released. Since the latter are much smaller than the elastic volume strains, the hysteresis loop of the volume is almost closed (within the accuracy of the present diffraction method). The width of the hysteresis loop is presumably determined by the shear strength of the pressure-transmitting medium relative to that of the sample. The complete relaxation of volume strains and stresses in NaCl reflects the behaviour of a perfectly plastic solid.

The pressurization of Cu_3Au after the first pressure cycle must reflect the compression behaviour of a plastically deformed solid. Hence, stages I and II should be absent, and only the last part of stage III and stage IV should be observed. Although there are only two compression points for this cycle, the first one at around 1 GPa shows a volume essentially unchanged from that at ambient conditions (representing the later parts of stage III), while the second one lies on the decompression curve above the discontinuity (stage IV).

It has been emphasized throughout this paper that the pressure recorded from ruby or NaCl represents a confining pressure. Since foils represent the limiting case of a non-ideal powder and are sometimes used as pressure markers, it is of interest to analyze what pressure would be recorded from such a foil. This question has been addressed by Meng, Weidner & Fei (1993) who used elasticity theory to show how the pressure calculated from a gold foil in neon can be corrected for uniaxial stresses. Since the equations derived by Singh (1993) are based on the theory of linear elasticity, their validity is strictly limited to elastic deformations. No attempt is made here to calculate a hydrostatic pressure from Cu_3Au since plastic deformation starts at very low pressures. The measured strain (from which the stress is calculated) above the yield point includes both the elastic and plastic strains. As shown here, the equations of Singh (1993) give reasonable values for the stress also in the case of plastic deformation. The influence of stacking faults on line shifts is discussed by Otto, Vassiliou & Frommeyer (1997*a*,*b*).

5. Conclusions

The compression of a polycrystalline elastically anisotropic material in an opposed-anvil device consists of the following stages:

Stage I: the sample is compressed elastically as long as the shear stresses transmitted by the pressure-transmitting medium are below the yield stress of the sample. For Cu_3Au this is about 1 GPa confining pressure in NaCl. Preliminary results from compression of a Cu_3Au foil in other pressure-transmitting media indicate that the yield point is reached at confining pressures of about 6 GPa in a 4:1 methanol–ethanol mixture and 3–4 GPa in paraffin oil [full details are to be given elsewhere (Otto, Vassiliou & Frommeyer, 1997*a*,*b*)]. It coincides with the yield strength of NaCl and an increase in the viscosity of 4:1 methanol–ethanol and of paraffin oil above some unknown value.

Stage II: as plastic deformation sets in due to the shear stresses transmitted, volume compression also continues as long as it is not prevented by the repulsion between the defects introduced. The compressibility is less than in stage I.

Stage III: volume compression is stopped by repulsion between defects. External stresses continue to build up. The range of constant volume with increasing confining pressure is determined by the shear strength of the pressure medium relative to the sample.

Stage IV: when the external pressure overcomes the repulsion between defects, volume compression continues: it is the elastic compression of a plastically deformed material. The transition from stage III to IV is marked by a discontinuity in the compression curve. It is caused, in the case of Cu_3Au, by the final solidification of a 4:1 methanol–ethanol mixture (at ~12 GPa) and of paraffin oil (~7 GPa) (Otto, Vassiliou & Frommeyer, 1997*a*,*b*).

On pressure release the elastic volume strains are recoverable (Fig. 2) with a hysteresis which is determined, for the same sample material, by the stress relaxation in the pressure medium. Plastic volume strains are not recoverable but are too small to be measured in the present experiments. On second pressurization the compression behaviour is due to stages III and IV only.

NaCl is not a suitable pressure medium for ductile (soft) materials. It begins to transmit shear stresses even at very low pressures. The confining pressure at which stresses in NaCl saturate and the maximum stress determined here agree very well with previous determinations of pure NaCl in an opposed tungsten carbide anvil cell (Singh & Kennedy, 1976), an ungasketted diamond-anvil cell (Kinsland & Bassett, 1977; Wu & Bassett, 1994), and cubic anvil devices (Weidner, Wang, Meng & Vaughan, 1994*b*; Otto, Vassiliou & Frommeyer, 1997*c*, who used both pure NaCl and NaCl enclosing a Ni_3Al foil). In all of these studies the Reuss state was assumed. It should be emphasized that the effects observed occur at well defined confining pressures only if the sample consists of a continuous network of crystals (a foil rather than a powder).

JWO would like to thank Professor W. B. Holzapfel for the loan of a diamond-anvil cell.

References

Birch, F. (1938). *J. Appl. Phys.* **9**, 279–288.
Decker, D. L. (1971). *J. Appl. Phys.* **42**, 3239–3244.
Funamori, N., Yagi, T. & Uchida, T. (1994). *J. Appl. Phys.* **75**, 4327–4331.
Kinsland, G. L. & Bassett, W. A. (1977). *J. Appl. Phys.* **48**, 978–985.
Mao, H. K., Bell, P. M., Shaner, J. W. & Steinberg, D. J. (1978). *J. Appl. Phys.* **49**, 3276–3283.
Meng, Y., Weidner, D. J. & Fei, Y. (1993). *Geophys. Res. Lett.* **20**, 1147–1150.
Otto, J. W. (1997*a*). *Nucl. Instrum. Methods*, A**384**, 552–557.
Otto, J. W. (1997*b*). *J. Appl. Cryst.* Submitted.
Otto, J. W., Vassiliou, J. K. & Frommeyer, G. (1997*a*). *J. Appl. Phys.* Submitted.
Otto, J. W., Vassiliou, J. K. & Frommeyer, G. (1997*b*). *Phys. Rev. B.* Submitted.
Otto, J. W., Vassiliou, J. K. & Frommeyer, G. (1997*c*). In preparation.
Piermarini, G. J., Block, S. & Barnett, J. D. (1973). *J. Appl. Phys.* **44**, 5377–5382.
Poirier, J. P. (1985). *Creep of Crystals*. Cambridge University Press.
Sato, Y., Yagi, T., Ida, Y. & Akimoto, S. (1975). *High Temp. High Press.* **7**, 315–323.
Siegel, S. (1940). *Phys. Rev.* **57**, 537–545.
Singh, A. K. (1993). *J. Appl. Phys.* **73**, 4278–4286.
Singh, A. K. & Kennedy, G. C. (1974). *J. Appl. Phys.* **45**, 4686–4691.
Singh, A. K. & Kennedy, G. C. (1976). *J. Appl. Phys.* **47**, 3337–3340.
Singh, A. K., Vijayan, K., Xia, H., Vohra, Y. K. & Ruoff, A. L. (1992). *Proceedings of the XIII AIRAPT/APS Conference on High-Pressure Science and Technology 1991*, edited by A. K. Singh, pp. 782–785. New Delhi: Oxford and IMH Publishing.
Spetzler, H., Sammis, C. G. & O'Connel, R. J. (1972). *J. Phys. Chem. Solids*, **33**, 1727–1737.
Syassen, K. & Holzapfel, W. B. (1975). *Europhys. Conf. Abstr.* **1A**, 75.
Vassiliou, J. K., Otto, J. W. & Porter, R. F. (1994). *Proceedings of the XIV AIRAPT/APS Conference on High-Pressure Science and Technology*, edited by G. Schmidt, J. W. Shaner, M. Nicol & M. Ross, pp. 461–464. New York: American Institute of Physics.
Weidner, D. J., Wang, Y., Meng, Y. & Vaughan, M. T. (1994*a*). *Proceedings of the XIV AIRAPT/APS Conference on High-Pressure Science and Technology*, edited by G. Schmidt, J. W. Shaner, M. Nicol & M. Ross, pp. 1025–1029. New York: American Institute of Physics.
Weidner, D. J., Wang, Y., Meng, Y. & Vaughan, M. T. (1994*b*). *J. Geophys. Res.* **21**, 753–756.
Wu, T. & Bassett, W. A. (1994). *Proceedings of the XIV AIRAPT/APS Conference on High-Pressure Science and Technology*, edited by G. Schmidt, J. W. Shaner, M. Nicol & M. Ross, pp. 1625–1629. New York: American Institute of Physics.
Yamaguchi, M. & Umakoshi, Y. (1990). *Progr. Mater. Sci.* **34**, 1–148.